Article

Journal of
Nanoscience and Nanotechnology
Vol. 15, 3004–3010, 2015
www.aspbs.com/jnn

Raman-Based Steady-State Thermal Characterization of Multiwall Carbon Nanotube Bundle and Buckypaper

Man Li and Yanan Yue*

School of Power and Mechanical Engineering, Wuhan University, Wuhan, 430072, China

Electrical methods for thermal characterization, like 3ω method,[1] micro-bridge method[2] and TET method,[3] have been widely used in the thermal property measurement, while always been limited by the electrical conductance of samples or other temperature dependent thermal resistors. As an optical method, Raman thermometry has been developed and broadly applied in thermal characterization in recent years. In this work, we present a steady-state method based on Raman spectroscopy for the localized thermal characterization of micro/nanowires and thin film materials, respectively. The physical models are developed and two kinds of materials: a MWCNT bundle and a piece of buckypaper are measured to validate this method. The thermal conductivities are measured as 4.92 W/m K and 0.83 W/m K for CNT bundle and buckypaper respectively. Compared with other optical methods, this steady-state Raman method features easy and fast way for thermal characterization, being capable of measuring samples from millimeters down to nanometers.

Keywords: Raman Spectroscopy, Steady State, Thermal Conductivity, Carbon Nanotube Bundle, Buckypaper.

1. INTRODUCTION

Emergence of new nanostructured materials brought up the huge demand for the thermal characterization which has higher standards due to the unique property as well as the tiny sizes of the materials. Existing micro/nanoscale thermal characterization techniques can be divided into electrical method and optical method by measurement tools and principle, as well as steady-state method and transient method from the time domain. Frequently used electrical methods, such as micro-bridge,[2,4] 3ω[1,5] and TET[3] are all based on the temperature dependence of electrical resistance. Calibration experiment for the relationship between temperature and resistance need to be established in advance of the measurement experiment. For samples with low temperature-resistance response or with rough surface which has difficulty in gold coating, the calibration experiment is difficult to accomplish. For samples with good optical absorption, the optical thermal characterization method is a better choice. Some methods such as laser flash[6,7] and pump-and-probe[8,9] are either based on the laser absorption or temperature dependence of reflectivity. They are all transient methods which have higher system requirements for coordination between excitation and probing.

In recent years, a steady-state optical method: the Raman thermometry technique has been widely used in thermal characterization of many materials,[10–14] including temperature coefficient characterizations of carbon nanotube and graphene,[15–18] temperature mapping in silicon-based electronics,[19] and so on. Very influential works include the first study of thermal conductivity of suspended single layer graphene by Balandin et al.[11] and another graphene measurement work by Lee et al.[20] Chen et al.[21] also used Raman method to study the thermal property of graphene in both vacuum and gaseous environments, which extensively prove the measurement capacity for nano-scale samples. In Raman thermometry, the peak frequency is often used as the temperature indicator due to the higher sensitivity than other features. For carbon materials which have been studied extensively in recent years, the Raman peak (e.g., *G*-band) shifts to the left as temperature increases, with a linear relationship within a small temperature range.[18] The peak intensity is also dependent on the temperature but usually get affected by the focal level of the sample. The temperature dependence of peak width is not as significant as two features above, but it is still a good reference for temperature probing because only

*Author to whom correspondence should be addressed.

 1533-4880/2015/15/3004/007 doi:10.1166/jnn.2015.9641

this feature is independent of strain effect.[22] The selection of Raman thermometry feature depends on the experimental conditions, such as the quality of materials, resolution limit of spectrometer and the specification of the probing laser. As a non-contact and non-destructive measurement approach, Raman thermometry is capable of monitoring temperature and characterizing the thermal property of sample with dimension down to nanometers.[19]

In our previous work, we developed a technique based on Raman thermometry to measure thermal conductivity of micro/nano wires, which is designated as the "Steady-state Electro-Raman-thermal, SERT" technique.[23,24] The SERT technique combines the Joule heating and Raman thermometry to measure the middle temperature to derive the thermal conductivity of the one-dimensional material. In that method, we eliminated the heating effect from incident laser by conducting the calibration experiment. As the matter of fact, the heating effect from the laser could be significant due to the small laser spot and powerful laser intensity to excite Raman signal. The heat dissipation from the laser absorption could be dominant in the laser irradiation area. Therefore, the study of localized heat dissipation at that point can be very interesting beside the uniform Joule heating along the sample. In this work, we report the modified SERT technique by eliminating the Joule heating and only considering heating effect from the laser. Without the need for nanofabrication of experiment circuit for Joule heating, this work features the fast and easy measurement, while being capable of measuring sample down to sub-micron size.

2. EXPERIMENTAL PRINCIPLE AND PHYSICAL MODEL DEVELOPMENT

2.1. Experimental Principle

The experiment principle is similar to SERT technique.[23] For micro/nanowires, the sample is bridge-suspended on two bulk heat sinks with ends closely pasted. In this technique, the ends' connections are used only for the heat dissipation purpose, thus the heat sink doesn't have to be metals. The incident laser is irradiated on the middle of the sample. Absorbed laser in the sample heats the irradiation spot, and the heat dissipates along the sample toward the ends. The endpoint temperature can be regarded as room temperature since the ends are attached on the bulk with large heat capacity. During laser heating experiment, the corresponding Raman signal is collected. Based on the Raman thermometry, the middle temperature of the sample can be obtained, thus the relationship between heating energy and temperature response can be established. The thermal conductivity of sample can be calculated according to this linear relationship, which will be discussed in details next for the physical model development.

For the thin film material, the sample is suspended on a hole with the edge closely attached on the substrate. Similar as aforementioned microwire experiment, the laser is irradiated on the center of the sample, and heat dissipates from the center to the edge. The local temperature at the center can be monitored by the corresponding Raman signals at different heating levels. Similar physical model is established with thermal conductivity readily derived from the linear relationship between the temperature rise and laser heating.

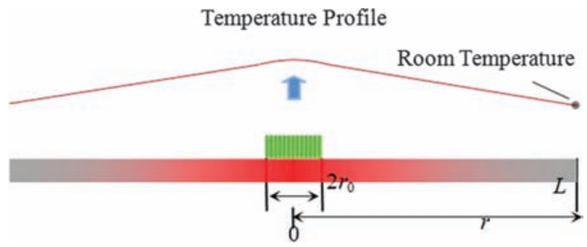

Figure 1. Experiment principle for thermal property measurement of micro/nanowires. Laser is irradiated on the middle point of the sample. Raman signal is collected to monitor its temperature rise.

2.2. Physical Model for Measuring Thermal Conductivity of Micro/Nanowires

Figure 1 shows the experimental principle of thermal property measurement of micro/nanowires. Assuming the thermal properties stay constants within a small temperature range, the governing equation for this 1-Dimentional steady-state model within laser irradiated region is: $k\Delta T + \dot{q} = 0$. In this equation, T is temperature, k is thermal conductivity of the material, $\dot{q}$ is equivalent heat generation rate (W/m^3) in the sample. It can be derived from the laser absorption Q as $\dot{q} = Q/2\pi r_s^2 r_0$, where r_s is radius of sample, r_0 is half length of laser beam. Outside laser heating region, the governing equation can be simplified as one without heat generation, that is $-kA\Delta T = Q/2$ since the heat dissipates in two directions towards the ends.

In laser irradiation area ($r < r_0$, r_0 is the half length of laser beam), combining with heat dissipation equation outside the laser irradiation region, the temperature distribution can be easily obtained by applying boundary conditions that end temperature of the sample is room temperature and there is no heat flux at $r = 0$ as:

$$T(r) = -\frac{Q}{4\pi k r_0 r_s^2} r^2 + \frac{Q}{2\pi k r_s^2}\left(L - \frac{r_0}{2}\right) + T_0$$

Thus, the average temperature within laser irradiation region can be derived as:

$$\overline{T} = \frac{1}{r_0}\int_0^{r_0} T(r)dr = \frac{QL}{2\pi k r_s^2} - \frac{Qr_0}{3\pi k r_s^2} + T_0$$

It shows that the average temperature at the laser heating area has the linear relationship with absorbed laser energy, and the coefficient is $(L/2\pi r_s^2 - r_0/3\pi r_s^2)/k$. Temperature can be directly measured from the Raman signal. Thus, the thermal conductivity of the micro/nanowires can be readily derived.

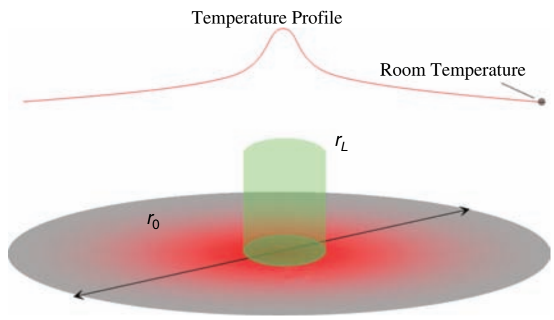

Figure 2. Experiment principle for thermal property measurement of thin film. Laser is irradiated at the center of the sample, heat dissipates to the edge. Raman signal is collected to monitor the localized temperature increase.

2.3. Physical Model for Measuring Thermal Conductivity of Thin Films

Similar as micro/nanowires, Figure 2 shows the measurement principle of thermal characterization of thin films. Assuming the thermal properties stay constants within a small temperature range and only steady-state heat conduction is considered, the governing equation for this two-dimensional heat dissipation model within laser irradiated region is: $k(1/r)(d/dr)(r(dT/dr)) + \dot{q} = 0$. In this equation, T is temperature, r is distance from the midpoint in radius direction of the sample, k is thermal conductivity of the material, and $\dot{q}$ is the equivalent heat generation rate ($Q/\pi r_0^2 d$, where r_0 is equivalent radius of laser irradiation area, d is thickness of the sample). Outside the laser heating area, the governing equation is $-kAdT/dr = Q$, where r is radius of the sample; A is cross-sectional area of the sample for the heat dissipation from the center to the margin.

For the region $r < r_0$: temperature distribution can be derived as:

$$T(r) = \frac{Q}{4k\pi r_0^2 d}(r_0^2 - r^2) + \frac{Q}{2k\pi d}(\ln r_L - \ln r_0) + T_0$$

Thus, the average temperature in laser irradiation area is:

$$\begin{aligned}\bar{T} &= \frac{1}{\pi r_0^2}\int_0^{2\pi} d\varphi \int_0^{r_0} rT(r)dr \\ &= \frac{Q}{k}\left[\frac{1}{8\pi d} + \frac{1}{2\pi d}(\ln r_L - \ln r_0)\right] + T_0\end{aligned}$$

It also shows that the average temperature at laser irradiation area has the linear relationship with laser energy (Q), and the coefficient is $[(\ln r_L - \ln r_0)/2 + 1/8]/\pi dk$. The center temperature can be directly measured from the Raman signal. Then, the thermal conductivity of the micro/nanowires can be obtained.

3. EXPERIMENTAL DETAILS AND DISCUSSION

3.1. Experimental Details

To validate this method, we use two samples for the thermal characterization. Figure 3 shows the experimental setup for

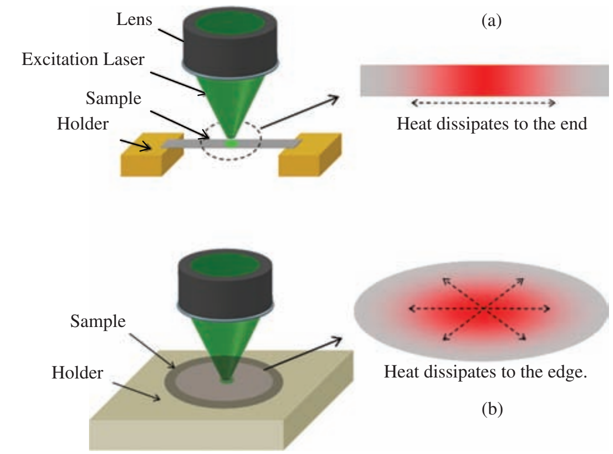

Figure 3. Experimental setup for 1-D(a), 2-D(b) thermal conductivity measurement.

thermal conductivity measurements of micro/nanowire (a), and thin film (b). In the micro/nanowire experiment, the multi-wall carbon nanotube bundle (MWCNT) from Oak Ridge National Laboratory is measured. The sample wire is torn from the original bundle with 1.57 mm in length and 0.07 mm in diameter (as shown in Fig. 4). Then it is suspended with two ends connected to the bulk materials. Raman spectrometer used in this work is installed with 532 nm excitation laser and a spectrometer with a 1.75 cm^{-1} pixel resolution. The full energy of the excitation laser is 20 mW. For carbon materials, the laser absorption at this wavelength is about 83%.[25] In the experiment, the 50X lens with long working distance is used for Raman signal collection. The focal plane of the laser beam through this lens is 2 μm (width) × 4 μm (length). To get sound Raman signal, an integration time of 240 seconds is used throughout the whole experiment. During the measurement, the laser is adjusted to focus on the middle, and 25%, 79% and 100% of the laser energy are used to heat the sample with Raman spectrum collected for corresponding temperature increase.

In the 2-D experiment, multiwall carbon nanotube thin film (named buckypaper) was used, as shown in Figure 5.

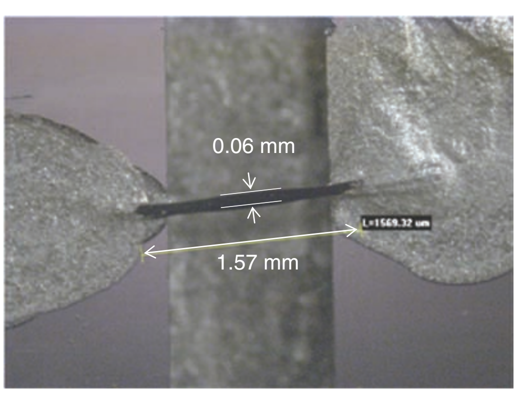

Figure 4. Sample image of CNT bundle, the total length is 1.57 mm and the width of sample is measured as 0.06 mm.

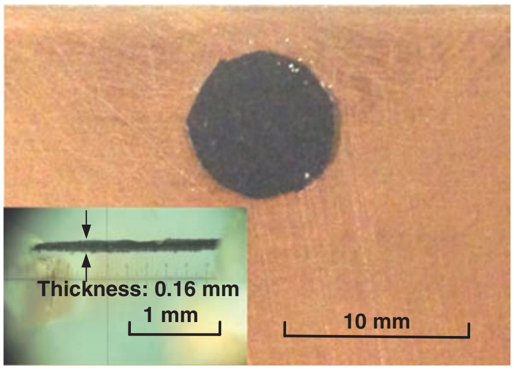

Figure 5. Sample image of CNT thin film (buckypaper), the diameter is 5 mm and the thickness[24] is 0.16 mm. Copyright Elsevier. Reproduced from reference with permission.

The sample was purchased from the NanoLab Inc. In the fabrication, MWCNTs (95%) are fully dispersed in the water for chemical treatment, then mixed with glue and pressurized to a black piece of paper. After it is dried, it is cut to different shapes for different applications. The sample used in this experiment is a small piece with 5 mm in diameter and 0.16 mm in thickness. The sample is placed on a copper piece with a hole just below the buckypaper piece. The edge of the sample is adhered to the copper for heat dissipation. Since the copper piece is big compared with the sample, it is reasonable to regard the edge temperature of the sample stays at room temperature. In the experiment, the same probing laser used in 1-D measurement is employed to focus on the center of the sample by using the 50X lens. Also, four energy levels: 25%, 79% and 100% of the laser energy are used to heat the sample with each Raman spectrum collected for corresponding temperature increase.

3.2. Experimental Result and Discussion

Figure 6(a) shows the typical Raman spectrum of MWCNTs (used in our experiment). Since the buckypaper is also made of MWCNTs, only one is shown here as an example. In this figure, we can clearly observe two distinct peaks: *D*-band (around 1350 cm^{-1}) and *G*-band (around 1590 cm^{-1}) for the range from 1000 cm^{-1} to 2000 cm^{-1}. The *D*-band peak stands for the structural defect in the carbon–carbon structures, people use *D*-band to qualify the structural quality of carbon nanotubes.[26] While the *G*-band is the graphite mode, comes from the planar vibrations of carbon atoms.[26] For most Raman thermometry study of carbon nanotubes, *G*-band is selected to study due to the sound signal and temperature response.[14] As shown in Figure 6(b), the temperature dependence for *G*-band is almost linear with coefficient -0.026 cm^{-1}/K, which has been confirmed by many researchers.[12,14] Figure 7(a) shows the Raman spectra of the CNT bundle at different heating levels. An obvious trend of blue shift of Raman peak (*G*-band) can be observed which means that there

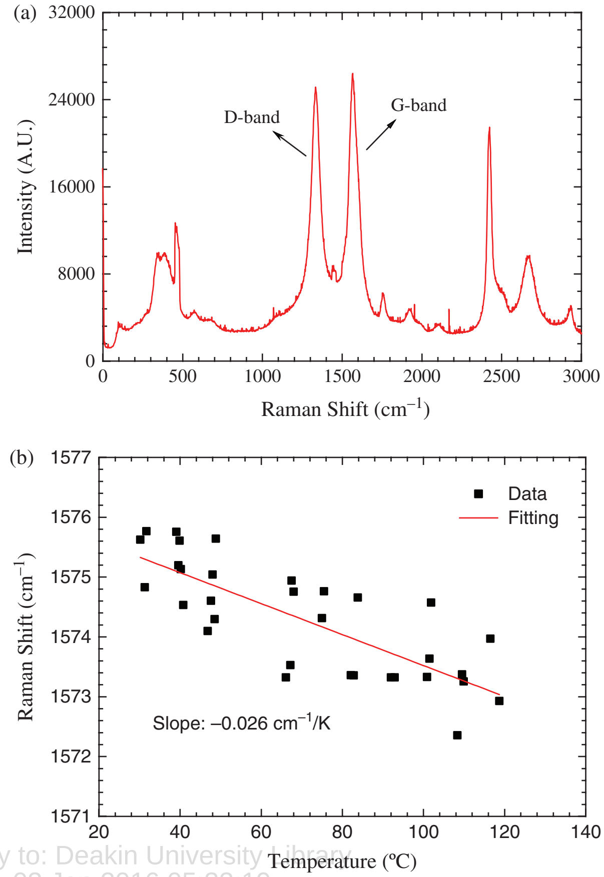

Figure 6. (a) Raman spectrum of multiwall carbon nanotube; (b) Calibration experiment for temperature dependence of *G*-band.

is sound temperature response when the higher heating intensities are applied. In all Raman thermometry experiments, there has been a problem about how to define the Raman spectrum at room temperature. Because there always involves the heating effect from probing laser despite how small the laser energy is, the local temperature of the sample is not actually the room temperature. To avoid this undesired heating effect, we didn't define the Raman spectrum at room temperature, but reasonably use a given Raman shift of *G*-band at room temperature. By using this value, the temperature rise for each heating level can be derived from the temperature coefficient of *G*-band aforementioned above. Figure 7(b) shows the relationship between temperature rise and heating power. The linear fitting is conducted. Since only the slope of the temperature-heating power relationship is counted for the thermal conductivity calculation, it doesn't matter what the Raman shift at room temperature has been used as long as the point at zero heating level is not involved in the fitting. Applied with the slope of linear fitting, the thermal conductivity of the sample can be derived from the slope as 4.09 W/m K.

Similar as the CNT bundle, the experimental result for buckypaper is shown in Figures 8(a) and (b). Figure 8(a) shows the Raman spectra at different heating levels.

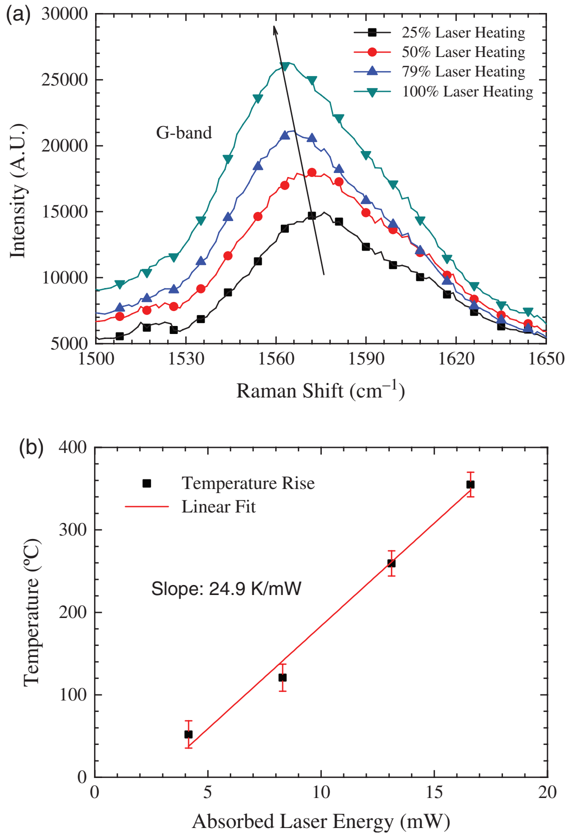

Figure 7. (a) Raman spectra of the CNT bundle at different laser heating levels; (b) Relationship between laser heating energy and corresponding temperature response. The linear fitting is conducted with slope as 24.9 K/mW.

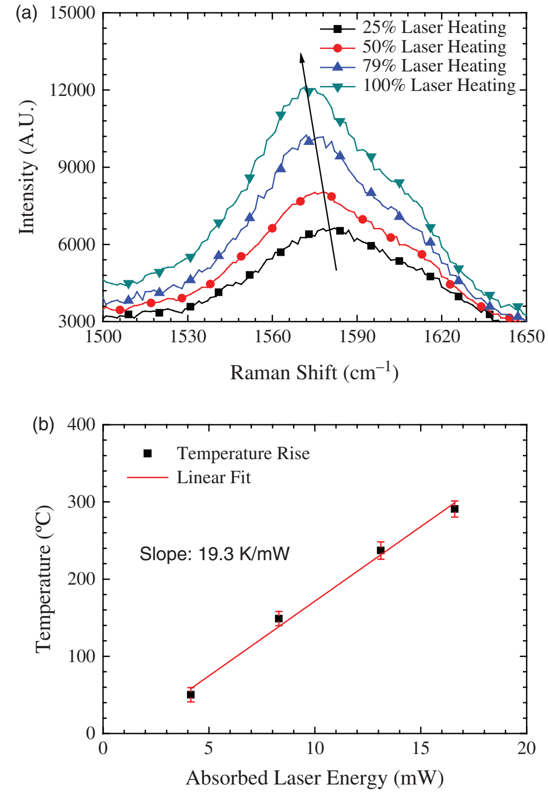

Figure 8. (a) Raman spectra of the CNT buckypaper at different laser heating levels; (b) Relationship between laser heating energy and corresponding temperature response. The linear fitting is conducted with slope as 19.3 K/mW.

An obvious trend of blue shift of *G*-band peak is observed. Applied the temperature coefficient for *G*-band, the relationship between temperature rise and heating power is established, as shown in Figure 8(b). In 2-D heat dissipation model for thin films, the thermal conductivity of the sample can be derived as 0.69 W/m K.

Comparing thermal conductivities of these two nanostructures, the MWCNT bundle has higher thermal conductivity than the buckypaper. Although they are all made of MWCNTs, the inner thermal property of the material is not just determined by the kind of material inside, but also highly dependent on the arrangement of inner materials. As shown in Figure 9 for the SEM images of two samples, the CNTs are randomly distributed in the buckypaper, while the CNTs are very good aligned inside the bundle. As known worldwide, the CNT dissipates heat very fast, with thermal conductivity in orders of 1000 W/m K,[27,28] it can be concluded that the main thermal resistance of our materials comes from the contact resistance of CNT-CNTs. In 2009, Chalopin et al. presented theoretical thermal analysis of pellets composed of micrometers-long CNTs by using Green functions.[29] They pointed out that there exists a limit in the order of a few W/m Ks for the thermal conductivity of CNT bucky materials due to the random distribution and the contact resistance effect inside the material.[29]

3.3. Error Analysis Due to Radiation and Convection Heat Loss

To avoid the measurement error from the heat loss induced by the radiation and convection effect, it is recommended to conduct the experiment in the vacuum environment supplied with additional self-heating setup to avoid radiation. But this also increases the complexity of the measurement system. Our experiments were conducted in the air rather than in the vacuum condition. In the following content, we will discuss the error induced by the thermal radiation and convection effect in the measurements.

For the CNT bundle, we can calculate the thermal radiation and convection heat loss at the highest heating level. It is good to approximate the temperature distribution as linear along the axis of CNT bundle with maximum at the middle point (T_m) since the laser irradiation area is much smaller than the rest. Assuming that the average temperature of the sample is $T_a = (T_m + T_0)/2$ and the emissivity of the sample surface is 1 (ideal black body), the thermal radiation can be simply estimated by $Q_r = \varepsilon\sigma A(T_a^4 - T_0^4)$ as 0.83 mW, where ε is emissivity factor (we used 1, the maximum value), σ is Stefan–Boltzmann

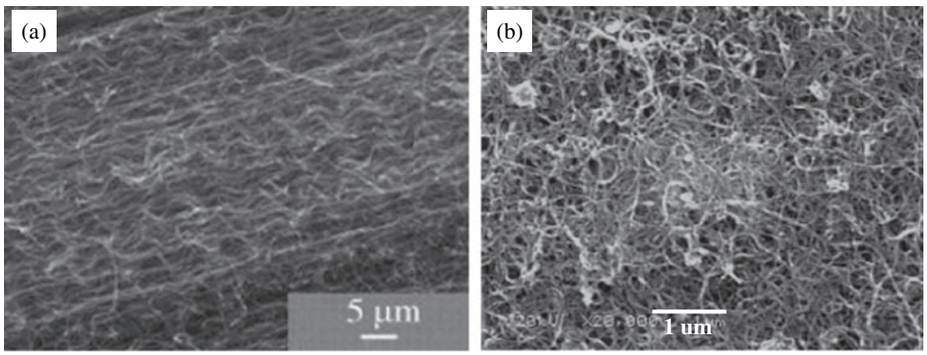

Figure 9. SEM images of (a) MWCNT bundle,[30] copyright Elsevier, reproduced with permission, and (b) buckypaper,[24] copyright Elsevier, reproduced with permission.

constant (5.67×10^{-8} W/m^2 K^4), A is the surface area of the sample. Compared with laser absorption (16.6 mW), the uncounted heat loss due to radiation only give an error about 5.22% on the thermal conductivity determination in the experiment. For the heat convection, the heat loss can be roughly calculated by $Q_c = hA(T_a - T_0)$ as 0.62 mW, where h is the coefficient for the nature heat convection (around 10 W/m^2 K). Compared with laser absorption, the uncounted heat loss due to radiation only give an error about 3.88% on the thermal conductivity result. The combined effects of thermal radiation and convection heat loss have the maximum error of 9.11% on the final result, which would not significantly decrease the measured value for the CNT bundle.

As the same analysis for the CNT bundle, we can calculate the thermal radiation and convection heat loss for the buckypaper. The temperature distribution in the radial direction of the sample can be written as $T(r) = -37.86 \ln(r/2.5 \times 10^{-3}) + 293$. Thus, the average surface temperature of the sample can be calculated by $\bar{T} = 1/\pi r_L^2 \cdot \int_0^{2\pi} d\varphi \int_{r_0}^{r_L} rT(r)dr$ as 312 K (at the maximum heating power). Assuming that the emissivity of the sample surface is 1 (ideal black body), the thermal radiation can be simply estimated by $Q_r = \varepsilon\sigma A(T_a^4 - T_0^4)$ as 4.67 mW, where ε is emissivity factor, σ is Stefan–Boltzmann constant (5.67×10^{-8} W/m^2 K^4), A is the surface area of the sample. Compared with total laser energy, the uncounted heat loss from radiation would give an error about 28% on the thermal conductivity. It is a reasonable result comparing with the CNT bundle since the buckypaper has much higher surface area than that. For the heat convection, the heat loss can be calculated by $Q_c = hA(T_a - T_0)$ as 7.43 mW, where h is the coefficient for the nature heat convection (assume 10 W/m^2 K). Compared with laser absorption, the uncounted heat loss due to radiation would give an error as high as 45% on the thermal conductivity evaluation. The combined effects of thermal radiation and convection heat loss have the significant error about 73%. Thus, the thermal conductivity measured our experiment can be over-estimated by the maximum of 73%. The real thermal conductivity could be as low as 0.40 W/m K.

3.4. Comparison with Steady-State Electro-Raman-Thermal (SERT) Technique

Recently developed SERT technique has its advantages in thermal characterization by using Joule heating, which can be easily controlled for even heating along the sample.[23] But the Joule heating requires the sample to be well connected to the electrodes which increases the difficulty of circuit fabrication. Meanwhile, the electrode connections should be carefully prepared in case that the high electrical contact resistance at the end could give undesired heating effect, which cannot keep the sample ends staying at the room temperature and involve error in Joule heating of sample and thus in thermal conductivity determination. For the laser-heating Raman method as introduced in this work, there should be no concerns about the electrical contact resistance since only laser irradiation area is regarded as heat generation area.

During thermal characterization experiment by SERT technique, the undesired heating effect from the probing laser could bring errors to some extent. Because the Raman signal is relatively low comparing with other photon scatterings, the laser energy should be high enough to excite enough photon to get sound Raman signal, therefore, in the experiment people would like to adjust the laser at the highest level. This comes out the problem that the relatively high laser energy focused on a small region of the sample would even be more intense than the Joule heating level. The measured temperature is not actually the value induced by the Joule heating but the combined effect of Joule heating and laser heating. Although this undesired heating effect can be mainly eliminated by conducting the calibration experiment, very little inconsistency in focal levels between calibration and measurement could give high errors in temperature determination. In laser-heating Raman method, this would not bother anymore since only laser heating is applied and evaluated in the calculation. The temperature can be precisely determined.

There is drawback of this laser-heating Raman method. Since the laser absorption is involved in the thermal conductivity determination, the laser absorption should be precisely determined, otherwise, it would contribute direct

error in thermal conductivity determination. Therefore, if the absorption ratio of the sample at corresponding wavelength is unknown, one has to conduct a pre-experiment or theoretical calculations to determine it. For some experiments conducted in various environments/conditions, one has to consider the light loss if the laser has to penetrate the lens to heat sample.

3.5. Measurement Capacity of Samples with Dimension Down to Sub-Micron

This laser-heating Raman method can be applied on the measurement experiment of extremely small samples, e.g., samples with sub-micron size. In this case, the laser beam can fully cover the sample and the measured temperature would be the mean value. Assuming that the absorbed laser intensity is $\bar{q}$, the mean temperature can be derived as $\bar{T} = \bar{q}L^2/3k + T_0$, for micro/nanowires where L is half length of the wire, the slope ($L^2/3k$, slightly different with that of the buck materials) of linear relationship between heating power and mean temperature can be used to determine thermal conductivity. For the thin films with size less than 1 μm, the mean temperature of the sample can be obtained as $\bar{T} = \bar{q}r_L^2/8k + T_0$, where r_L is the effective radius of the sample (for example, the round sample). The slope: $r_L^2/8k$ can be used to determine thermal conductivity of the material.

4. CONCLUSION

In this work, a simple steady-state thermal characterization method based on Raman spectroscopy is presented for measuring thermal conductivity of micro/nanowires, and thin films. By irradiating at the center of the materials with probing laser, corresponding temperature rise can be monitored and used for calculating thermal conductivity based on physical models developed in this work. To validate this method, two typical samples: the MWCNT bundle and buckypaper are tested with thermal conductivity measured as 4.09 W/m K and 0.69 W/m K, respectively. The relatively low value for the buckypaper is attributed to the random distribution of inside CNTs, which gives the high contact resistance for the thermal transport. The measurement uncertainty is discussed for the heat loss due to the radiation and convection effect. Overall, this technique features easy and fast way for measuring thermal property, being capable of measuring sample with down to sub-micron scales.

Acknowledgments: The financial support from Start-up of Wuhan University and National Science Foundation of China (No. 51206124) are gratefully acknowledged. Y. Yue would like to thank Professor Xinwei Wang from Iowa State University for the great help on the convenient access to the lab equipment.

References and Notes

1. X. J. Hu, J. Xu, K. E. Goodson, T. S. Fisher, and A. A. Padilla, *J. Heat Transfer* 128, 1109 (**2005**).
2. P. Kim, L. Shi, A. Majumdar, and P. L. McEuen, *Phys. Rev. Lett.* 87, 215502 (**2001**).
3. J. Guo, X. Wang, and T. Wang, *J. Appl. Phys.* 101, 063537 (**2007**).
4. P. Kim, L. Shi, A. Majumdar, and P. L. McEuen, *Physica B* 323, 67 (**2002**).
5. J. H. Kim, A. Feldman, and D. Novotny, *J. Appl. Phys.* 86, 3959 (**1999**).
6. B. Tetsuya and O. Akira, *Meas. Sci. Technol.* 12, 2046 (**2001**).
7. W. N. dos Santos, P. Mummery, and A. Wallwork, *Polym. Test* 24, 628 (**2005**).
8. W. S. Capinski, H. J. Maris, T. Ruf, M. Cardona, K. Ploog, and D. S. Katzer, *Phys. Rev. B* 59, 8105 (**1999**).
9. B. C. Daly, H. J. Maris, A. V. Nurmikko, M. Kuball, and J. Han, *J. Appl. Phys.* 92, 3820 (**2002**).
10. S. Perichon, V. Lysenko, B. Remaki, D. Barbier, and B. Champagnon, *J. Appl. Phys.* 86, 4700 (**1999**).
11. A. A. Balandin, S. Ghosh, W. Bao, I. Calizo, D. Teweldebrhan, F. Miao, and C. N. Lau, *Nano Lett.* 8, 902 (**2008**).
12. I. K. Hsu, R. Kumar, A. Bushmaker, S. B. Cronin, M. T. Pettes, L. Shi, T. Brintlinger, M. S. Fuhrer, and J. Cumings, *Appl. Phys. Lett.* 92, 063119 (**2008**).
13. M. Balkanski, R. F. Wallis, and E. Haro, *Phys. Rev. B* 28, 1928 (**1983**).
14. F. Huang, K. T. Yue, P. Tan, S.-L. Zhang, Z. Shi, X. Zhou, and Z. Gu, *J. Appl. Phys.* 84, 4022 (**1998**).
15. L. Zhang, Z. Jia, L. Huang, S. O'Brien, and Z. Yu, *J. Phys. Chem. C* 112, 13893 (**2008**).
16. L. Song, W. Ma, Y. Ren, W. Zhou, S. Xie, P. Tan, and L. Sun, *Appl. Phys. Lett.* 92, 121905 (**2008**).
17. M. J. Allen, J. D. Fowler, V. C. Tung, Y. Yang, B. H. Weiller, and R. B. Kaner, *Appl. Phys. Lett.* 93, 193119 (**2008**).
18. I. Calizo, A. A. Balandin, W. Bao, F. Miao, and C. N. Lau, *Nano Lett.* 7, 2645 (**2007**).
19. M. R. Abel, T. L. Wright, W. P. King, and S. Graham, *IEEE T. Compon. Pack. T* 30, 200 (**2007**).
20. J.-U. Lee, D. Yoon, H. Kim, S. W. Lee, and H. Cheong, *Phys. Rev. B* 83, 081419 (**2011**).
21. S. Chen, A. L. Moore, W. Cai, J. W. Suk, J. An, C. Mishra, C. Amos, C. W. Magnuson, J. Kang, L. Shi, and R. S. Ruoff, *ACS Nano* 5, 321 (**2010**).
22. T. Beechem, S. Graham, S. P. Kearney, L. M. Phinney, and J. R. Serrano, *Rev. Sci. Instrum.* 78, 061301 (**2007**).
23. Y. Yue, G. Eres, X. Wang, and L. Guo, *Appl. Phys. A* 97, 19 (**2009**).
24. Y. Yue, X. Huang, and X. Wang, *Phys. Lett. A* 374, 4144 (**2010**).
25. D. R. Lide, CRC Handbook of Chemistry and Physics, Internet Version (87th edn.), Taylor and Francis, Boca Raton, FL (**2007**), pp. 12–117.
26. M. S. Dresselhaus and P. C. Eklund, *Adv. Phys.* 49, 705 (**2000**).
27. S. Berber, Y.-K. Kwon, and D. Tománek, *Phys. Rev. Lett.* 84, 4613 (**2000**).
28. M. Fujii, X. Zhang, H. Xie, H. Ago, K. Takahashi, T. Ikuta, H. Abe, and T. Shimizu, *Phys. Rev. Lett.* 95, 065502 (**2005**).
29. Y. Chalopin, S. Volz, and N. Mingo, *J. Appl. Phys.* 105, 084301 (**2009**).
30. X. Huang, J. Wang, G. Eres, and X. Wang, *Carbon* 49, 1680 (**2011**).

Received: 28 September 2013. Accepted: 16 January 2014.